JETIR.ORG ISSN: 2349-5162 | ESTD Year : 2014 | Monthly Issue
JOURNAL OF EMERGING TECHNOLOGIES AND INNOVATIVE RESEARCH (JETIR)
An International Scholarly Open Access, Peer-reviewed, Refereed Journal

Non-linear stretching surface effects on Darcy-Forchheimer MHD hybrid nanofluid flow subjected to non-linear thermal radiation and mixed convection

[1]Bikram Singh, [2]Shikha Chandel and [3]Shilpa Sood
[1]Research Scholar, [2]Assistant Professor and [3]Asscoiate Professor
[1]Department of Mathematics and Statistics
[1]Career Point University, Hamirpur, Himachal Pradesh-176041, INDIA

Abstract

The principal purpose of this research is to examine the flow behavior of the uniform 2-dimensional and incompressible natural convectional MHD hybrid nanofluid flow incorporating metal oxide (GO) and silver (Ag) suspended in water along a sheet stretching non-linear. A non-linear stretching sheet offers more conclusive prediction of the flow dynamics and thermal exchange attributes with diverse applications in Biomedical engineering, Aerospace engineering and sheet manufacturing. In order to make our model more versatile we incorporate porous media, thermal radiation and mixed convection with non-linear effect . Using mathematical transformations, the governing complex partial differential equations (PDEs) are simplified to non-linear ordinary differential equations (ODEs) of higher-order and then solved numerically. Our investigation utilizes graphical visualization generated by the bvp4c Matlab solver to comprehensively analyze the significant impact of various physical parameters on skin friction coefficient,temperature profiles, local Nusselt number and velocity profile. The results validation is also performed. The results show that factors like nanoparticles concentration, temperature ratio and radiation can significantly enhance the flow velocity. Conversely, factors like nonlinear stretching, porosity and magnetic field strength lead to velocity reduction. Heat transfer is augmented by parameters like nonlinear convection and buoyancy forces, while it diminishes with factors like nanoparticle concentration and magnetic field. Furthermore, the effect of the shape factor of nanoparticles is also discussed and the result favours spehrical-shaped nanoparticles over bricks and platlet shaped for better heat transfer rates, which validates the fact of favorable cooling under consideration of non-linear thermal radiation. Overall, the study contributes to a deeper understanding of convective heat transfer processes in nanofluids under mixed convection and magnetic field effects.

Introduction

Recently, the investigation of nanofluids has gained attention due to their extensive applications across diverse scientific fields, including heat exchangers, chemical industries, solar panels, biomedical instruments, cooling of electronics, nuclear reactor heat pipes and car radiators because of their excellent thermophysical properties (Singh et al., 2006; Nagarajan et al., 2014; Ahammed et al., 2016; Wong and De Leon, 2010). Nanofluids refer to the combination of nanoscale particles with a liquid (such as ethylene glycol (EG), oils, water). Choi and Eastman (1995) are credited with presenting the idea of nanofluids.Many researchers have recently conducted studies on nanofluid flow behavior with the primary goal of improving heat transfer (Mukherjee et al., 2018; Xuan and Li, 2000; Javadi et al., 2013). Eastman et al. (2001) used copper nanoparticles (NPs) to refine the thermal conductivity of EG. They found 40% amplification in conductive heat capacity with the inclusion of 0.3 vol% of copper nanoparticles in EG. Maiga et al. (2004) compared $water-\gamma Al_2O_3$ and $EG-\gamma Al_2O_3$ nanofluids for better heat transfer inside a heated tube. The result showed improvement in heat transmission with NPs inclusion and supported $EG-\gamma Al_2O_3$ over $water-\gamma Al_2O_3$.

In an attempt to push the boundaries of heat transfer, researchers have developed hybrid nanofluids (Hnfs) in the early 2000s. These novel fluids incorporate one or more distinct kinds of NPs into the base liquid. This approach offers the potential for significantly enhanced thermal performance compared to nanofluids (Modi et al., 2023; Xu et al., 2022; Hayat and Nadeem, 2017; Karaaslan and Menlik, 2021; Singh and Sood, 2024). Turcu et al. (2006) synthesised $MWCNTs-Fe_3O_4$ hybrid nanomaterial using polypyrrole polymerization. Jana et al. (2007) evaluated the effectiveness of amplifying fluid's thermal conductance through incorporation of mono and hybrid NPs . Suresh et al. (2011) fabricated Al_2O_3-Cu (90:10) NP composite utilizing the hydrogen reduction method and then suspended into water within 0.1 to 2% concentration range. The heat conduction and viscosity of Hnf found to escalate. Stability investigation of (magnetic hydrodynamics) MHD Al_2O_3-Cu/H_2O nanofluid with quadratic velocity profile near a stretching/shrinking sheet to be permeable in nature is investigated by Zainal et al. (2021). The wall shear stress acting on the shrinking sheet escalates with the augmentation in NP volume fraction. Nadeem et al. (2020) studied the flow behaviour of Hnf over stretched surfaces numerically using MATLAB. The results favour Hnf over nanofluid for better heat transmission. Khan et al. (2021) demonstrate the heat transmission properties and micro-rotation of a micropolar Hnf flowing on a

non-isothermal shrinking/stretching sheet. Micro-rotation decreases with rising NP volume fraction in first branch, whereas it increases in the second branch. Temperature, however, rises in both cases.

Nonlinear stretching sheet involvement holds paramount importance across industrial contexts, including polymer sheet manufacturing and geothermal energy extraction. Bearing this in consideration, researchers have devoted significant effort to understanding fluid flow behaviour on these sheets. Cortell (2007) studied transfer of heat within a viscous liquid traversing a non-linear stretching sheet numerically using the Runge–Kutta algorithm. Mustafa and Khan investigated thermal transmission in Casson nanofluid over nonlinear stretched sheet, considering the magnetic field effect and sheet temperature to be nonlinear. Examining the interplay of Eckert number and radiation on heat transfer, Fenuga et al. (2020) investigated a vertical sheet stretched non-linearly with MHD flow close to a stagnation-point area. Their analysis revealed that heightened flow temperature, Eckert number and radiation were correlated with reduced heat transfer rates at the surface. Bhatti et al. (2020) examined the thermal attributes of Hnf flow on a permeable sheet with non-linear stretching, considering the impact of Dufour and Soret diffusion phenomena.

Understanding mixed convection in a fluid flow is essential due to its wide range over variety of applications including electronic cooling, solar energy systems and industrial processes. Many investigations have been reported with linear mixed convection (Ramzan et al., 2021; Puneeth et al., 2021; Ali et al., 2022; Khan et al., 2020), but non-linear mixed convection also holds significant importance in a fluid's heat transport and flow behaviour. Ashlin and Mahanthesh (2019) studied the non-linear convective motion driven by the non-coaxial spinning of a planar plate around a vertical axis, employing three distinct fluids H_2O, $Al_2O_3-H_2O$ and $Cu-Al_2O_3-H_2O$. The visocus force and heat conduction of Hnf is reported to be superior to the other two liquids. Influence of non-linear mixed convection with fluid flow under Darcy-Forchheimer phenomenon over stretching surface with nonlinear inclination is studied by Hayat et al. (2020a). Afzal et al. (2023) explores a nanofluid based on blood comprising uranium dioxide, thorium dioxide and Radium. The fluid model depicts blood arteries, which are formulated using cylindrical coordinates and integrates porous medium, non-linear combined convection, temperature and velocity slip, non-linear radiative heat transfer and MHD effect.

Porous media flow has emerged as a critical research area due to its real-world applications from modeling blood flow, pollutant movement in aquifers, geophysics to designing heat transfer systems. The well-established Darcy model forms the foundation for analyzing fluid behaviour, with Forchheimer's extension incorporating inertial effects. Recent research focuses on applying Darcy-Forchheimer model to diverse liquid flows within porous media. Srinivasacharya and Surender (2015) analyzed the thermal and mass transport of a Newtonian fluid experiencing dual stratification effect with porous media inclusion through Darcy-Forchheimer model. Sadiq and Hayat (2016) examined magneto Maxwell fluid across a streching sheet in two-dimensional space. Hayat et al. (2020b) scrutinized the viscous dissipation and thermal transmission on flow of nanofluid around a rotated disk under the Darcy-Forchheimer model. Mallikarjuna et al. (2021) demonstrated a mathematical framework for dusty Hnf flow on a extended surface, taking consideration of viscous dissipation and melting effect within the Darcy–Forchheimer two-phase flow model. Haider et al. (2021) used Darcy-Forchheimer model to study how non-linear thermal stratification and radiation affect $TiO_2-Al_2O_3/water$ nanofluid.

Motivated by the literature review, the author aims to model and examine numerically the Darcy-Forchheimer $(GO+Ag)/H_2O$ Hnf across a sheet stretched non-linearly. The integrated consequence of non-linear thermal radiation and nonlinear mixed convection with magnetic field influence are also taken into model formulation. The flow properties of hybrid nano liquid comprising velocity, heat transmission rate, temperature and Friction drag coefficient are discussed through graphical representations and tabular data using bvp4c. To further explore the potential for performance optimization, this work delves into the impact of shape factor on NP behaviour, with a focus on heat transfer enhancement.

Mathematical description of the problem

Consider two-dimensional steady and non-compressible free convectional MHD Hnf, incorporating silver (Ag) and graphene oxide (GO) NPs flow over a surface under non-linear stretching, with the x-axis coinciding with the extending surface and the orthogonal axis to it is denoted by y. The flow is subject to significant buoyancy forces, resulting in non-linear convective flow within a permeable medium. A consistent magnetic influence of magnitude $B_0(x)$ is directed parllel to the orthogonal axis. Assuming a minimal magnetic Reynolds number for the fluid, we opted of ignoring the induced magnetic field in our analysis. Additionally, non-linear thermal radiation contributions are included. The stretched surface experiences a non-linear velocity profile U_w whose behaviour is determined by the constant b (>0) and the non-linear stretching parameter n. In view of outlined assumptions and integrating the Boussinesq approximations and boundary layer, the governing equations for continuity, momentum and energy formulated as follows

$$\frac{\partial u}{\partial x}+\frac{\partial v}{\partial y}=0, \tag{1}$$

$$u\frac{\partial u}{\partial x}+v\frac{\partial u}{\partial y}=\frac{\mu_{hnf}}{\rho_{hnf}}\frac{\partial^2 u}{\partial y^2}+g(\beta_{1hnf}(T-T_\infty)+\beta_{2hnf}(T-T_\infty)^2)-\frac{\nu_{hnf}}{k^*}u-\frac{c_b}{\sqrt{k^*}}u^2-\frac{\sigma_{hnf}}{\rho_{hnf}}B_o^2u \tag{2}$$

$$u\frac{\partial T}{\partial x}+v\frac{\partial T}{\partial y}=\frac{k_{hnf}}{(\rho c_p)_{hnf}}\frac{\partial^2 T}{\partial y^2}-\frac{1}{(\rho c_p)_{hnf}}\frac{\partial q_r}{\partial y}. \tag{3}$$

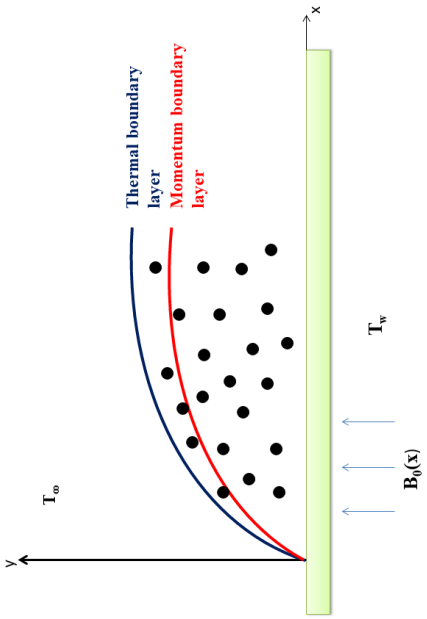

Figure 1: Flow configuration schematic diagram

With considered boundary constraints:

$$\left.\begin{array}{llll} u = U_w = bx^2, & v = 0, \quad T = T_w & at & y = 0, \\ u \to 0, T \to T_\infty & as & y \to \infty. & \end{array}\right\} \tag{4}$$

In x and y directions, u and v are stated as velocity elements respectively. T is the nanofluid's temperature, T_w and T_∞ ($T_w > T\infty$) are the sheet's and in the surrounding temperatures respectively, $\nu = \frac{\mu}{\rho}$ is kinematic viscosity, β_{1hnf} and β_{2hnf} are thermal linear and non-linear expansions and k^* signifies porous medium's characteristic of permeability. The parameter n, with n being non-negative, defines the extent of non-linear stretching of the sheet, while the sheet behaviour is linear for $n = 1$. Further heat capacity, thermal conductance, density and dynamic viscosity of Hnf correspondingly represented by $(\rho c_p)_{hnf}$, k_{hnf}, ρ_{hnf} and μ_{hnf} as mentioned in tables 1 and 2 in which ϕ_1 and ϕ_2 denotes graphene-oxide and silver concentration respectively and subscript f is fluid, $n1$ for GO, $n2$ for Ag, nf is nanofluid and hnf is hybrid nanofluid.

Table 1 GO and Ag thermal properties along with H_2O (Sheikholeslami et al., 2014; Masood et al., 2021)

Parameters	GO	Ag	Water
$\rho(kgm^{-3})$	1800	10500	997.1
$K(Wm^{-1}K^{-1})$	5000	429	0.613
$C_p(Jkg^{-1}K^{-1})$	717	235	4179
$\sigma(\Omega m)$	6500	3.60×10^7	0.05

Table 2 Hnf thermophysical properties (Thakur and Sood, 2023; Masood et al., 2021)

Properties	Nanofluid	Hnf
Density	$\rho_{nf} = (1-\phi_1)\rho_f + \phi_1\rho_{n1}$	$\rho_{hnf} = (1-\phi_2)[(1-\phi_1)\rho_f + \phi_1\rho_{n1}] + \phi_2\rho_{n2}$
Viscosity	$\mu_{nf} = \frac{\mu_f}{(1-\phi_1)^{2.5}}$	$\mu_{hnf} = \frac{\mu_f}{(1-\phi_1)^{2.5}(1-\phi_2)^{2.5}}$
Thermal conductivity	$k_{nf} = \frac{k_{n1} + 2k_f - 2\phi_1(k_f - k_{n1})}{k_{n1} + 2k_f + \phi_1(k_f - k_{n1})} k_f$	$k_{hnf} = \frac{k_{n2} - 2\phi_2(k_{nf} - k_{n2}) + 2k_{nf}}{k_{n2} + \phi_2(k_{nf} - k_{n2}) + 2k_{nf}} k_{nf}$
Electrical conductivity	$\sigma_{nf} = \frac{\sigma_{n1} + 2\sigma_f - 2\phi_1(\sigma_f - \sigma_{n1})}{\sigma_{n1} + 2\sigma_f + \phi_1(\sigma_f - \sigma_{n1})}(\sigma_f)$	$\sigma_{hnf} = \frac{\sigma_{n2} + 2\sigma_{nf} - 2\phi_2(\sigma_{nf} - \sigma_{n2})}{\sigma_{n2} + 2\sigma_{nf} + \phi_2(\sigma_{nf} - \sigma_{n2})}(\sigma_{nf})$
Heat capacity	$(\rho C_p)_{nf} = (\rho C_p)_{n1}\phi_1 + (\rho C_p)_f(1-\phi_1)$	$(\rho C_p)_{hnf} = [(\rho C_p)_{n1}\phi_1 + \rho C_p)_f(1-\phi_1)](1-\phi_2) + ($

The subsequent expression represents the radiative heat flux (Mahanthesh et al., 2019)

$$q_r = -\frac{4\sigma^*}{3K^*}\frac{\partial T^4}{\partial y} = -\frac{16\sigma^*}{3K^*}T^3\frac{\partial T}{\partial y}, \tag{5}$$

for clarity, K^* used here for the absorption coefficient and σ^* as Stefan-Boltzmann constant.

The approach utilized for similarity conversion involves (Eid et al., 2018)

$$\left.\begin{aligned} \psi(x,y) &= \left(\frac{2\nu_f b}{m+1}\right)^{\frac{1}{2}} x^{\frac{n+1}{2}} f(\eta), \theta(\eta) = \frac{T - T_\infty}{T_w - T_\infty}, \\ u &= axf'(\eta), v = -\left(a\nu_f\right)^{\frac{1}{2}} f(\eta), \eta = y\left(\frac{b(n+1)}{2\nu_f}\right)^{\frac{1}{2}} x^{\frac{n-1}{2}} \end{aligned}\right\} \tag{6}$$

f and θ represent the self-similar velocity and temperature respectively, in addition to η serving as dimensionless variable. The stream function ($\psi(x,y)$) termed as

$$u = \frac{\partial \psi}{\partial y} \qquad and \qquad v = -\frac{\partial \psi}{\partial x} \tag{7}$$

By utilizing Eqs. (4) - (7), Eq. (1) holds true spontaneously, while Eqs. (2) and (3) transformed to

$$\frac{\mu_{hnf}/\mu_f}{\rho_{hnf}/\rho_f} f''' - f'^2\frac{2n}{n+1} + ff'' + \frac{2\lambda}{n+1}\theta(1 + A_2\theta) - Kf' - f'^2\frac{2}{n+1}Fr - \frac{\sigma_{hnf}/\sigma_f}{\rho_{hnf}\rho_f}M^2 f' = 0, \tag{8}$$

$$\frac{K_{hnf}/K_f}{\left(\rho C_p\right)_{hnf}/\left(\rho C_p\right)_f}\theta'' + \frac{Nr}{\left(\rho C_p\right)_{hnf}/\left(\rho C_p\right)_f}\left[3\theta'^2(\theta_w - 1)\left[1 + (\theta_w - 1)\theta\right]^2\right] + \frac{Nr}{\left(\rho C_p\right)_{hnf}/\left(\rho C_p\right)_f}\theta''\left[1 + (\theta_w - 1)\theta\right]^3 + Prf\theta' = 0 \tag{9}$$

and

$$\begin{aligned} f(0) &= 0, f'(0) = \theta(0) = 1, \\ f'(\infty) &= \theta(\infty) = 0. \end{aligned} \tag{10}$$

with non-dimensional parameters as:

$$\lambda = \frac{Gr_x}{Re_x^2},\ Gr_x = \frac{g\beta_{1hnf}(T_w - T_\infty)x^3}{\nu^2},\ Re = \frac{U_w x}{\nu},\ A_2 = \frac{\beta_{2hnf}(T_w - T_\infty)}{\beta_{1hnf}},\ Nr = \frac{16\sigma^* T_\infty^3}{3k^* k_f},\ M^2 = \frac{2\sigma B_0^2}{\rho_f b(n+1)x^{n-1}},\ Fr = \frac{c_b x}{\sqrt{k^*}}$$

and $K = \frac{2\nu_{hnf}}{k^* b(n+1)x^{n-1}}$

The variations in heat transfer and shear stress are quantified by the local Nusselt and skin-friction coefficient numbers, defined as (Nandeppanavar et al., 2023):

$$Nu = \frac{\left(-K(\frac{\partial T}{\partial y}) + (q_r)\right)_{y=0}}{K(T_w - T_\infty)} \qquad and \qquad C_f = \frac{\left(\mu\left(\frac{\partial u}{\partial y}\right)\right)_{y=0}}{\rho U_w^2} \tag{11}$$

On reducing,

$$\left.\begin{aligned} Re^{1/2}C_f &= \left(\frac{n+1}{2}\right)^{\frac{1}{2}} f'''(0), \\ Re^{-1/2}Nu &= -\left(\frac{n+1}{2}\right)^{\frac{1}{2}} (1 + Nr\theta_w^3)\theta'(0). \end{aligned}\right\} \tag{12}$$

Numerical solution

This section outlines the methodology for solving ODEs $9-11$ through the utilization of the "bvp4c" function within the MATLAB software. Using a finite-difference algorithm, the "bvp4c" function adopts a three-stage collocation formula (Chandel and Sood, 2022; Kierzenka and Shampine, 2001). Employing following substitutions enables the conversion of the system of ODEs and associated boundary conditions are reformulated into a collection of differential equations of first-order.

$y_1 = f, y_2 = f', y_3 = f'', y_4 = \theta, y_5 = \theta'$.

At the initial mesh point, an early prediction must be tailored to align with the specified solutions. It's crucial to provide an appropriate initial trial assumption, and the boundary condition involving $\eta \to \infty$ is rounded to a finite value finite value, i.e. $\eta = 10$.

The MATLAB syntax employed for this process is represent in Figure 2 as :

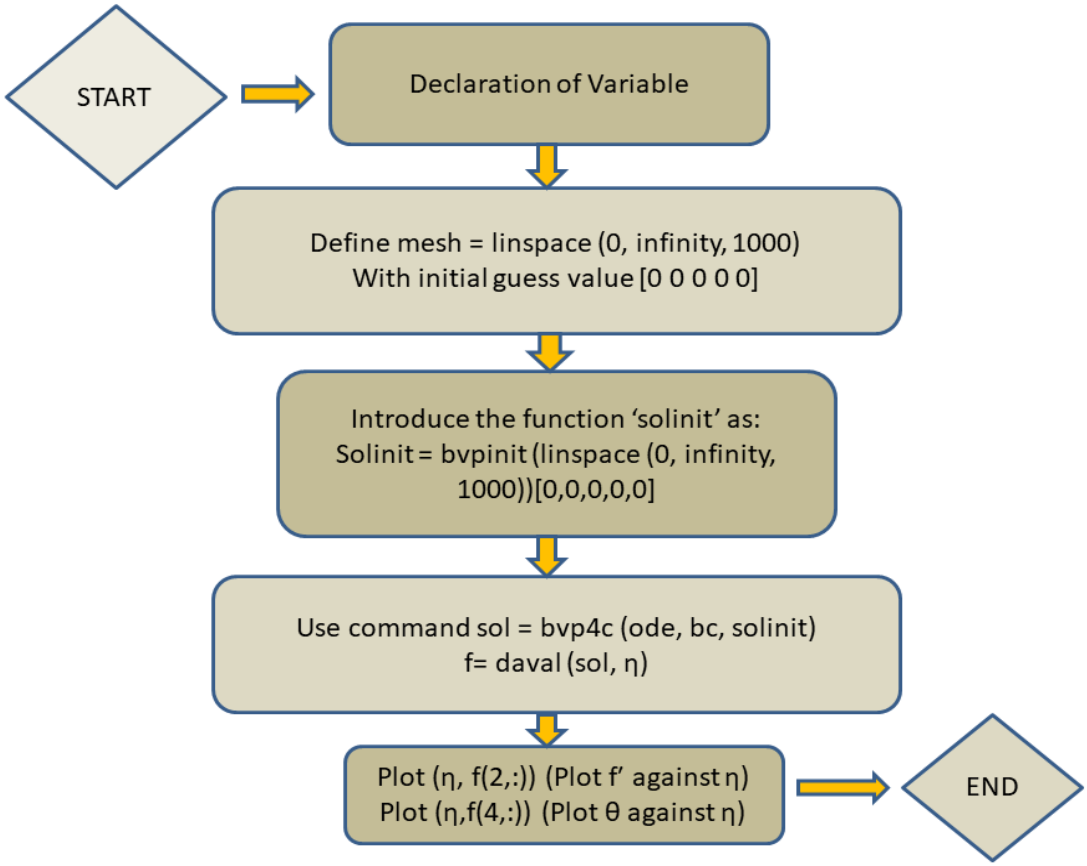

Figure 2: Visual Representation to the bvp4c Algorithm

Results and discussion

Here, we analyze the outcomes derived through numerical analysis and their corresponding physical interpretations. The effects of concentration parameter ϕ_1 (for GO) and ϕ_2 (for Ag), Forchheimer number (Fr), temperature ratio parameter (θ_w), Prandtl number (Pr), porosity parameter (K), non-linear convection parameter (A_2), non-linear radiation parameter (Nr), magnetic parameter (M), non-linear stretching parameter (n) and buoyancy parameter (λ) are investigated. In cases where parameters

exhibit a constant nature, the fixed values are set as follows: $Pr = 6.2$, $\theta_w = 1.5$, $n = 0.5$, $A_2 = Nr = 0.5$, $M = 0.5$, $\lambda = 1.0$, $K = 0.4$, $\phi_1 = \phi_2 = 0.3$ and $Fr = 0.5$. Table 3 compares- $\theta(0)$ and - $f''(0)$ values with those obtained from Cortell (2007) and Pandey et al. (2023) over a range of values for n, confirming the validity of the numerical technique that was used and showing a strong agreement.

Table 3 Analysis of the comparative findings related - $f''(0)$ and - $\theta(0)$ with $M = K = A_2 = Nr = \phi_1 = \phi_2 = Fr = \lambda = 0, \theta_w = Pr = 1$

n	**Present results for** - $f''(0)$	Cortell (2007)	Pandey et al. (2023)	**Present results for** - $\theta(0)$	Cortell (2007)	Pandey et al. (2023)
0.5	0.889552	0.889477	0.8895518	0.595223	0.595277	0.5952206
1.0	1.0	1.0	1.0	0.582010	-	-
1.5	1.061609	1.061587	1.0616092	0.574771	0.574537	0.5747719
3	1.148601	1.148588	1.1486013	0.564717	0.564472	0.5647180
10	1.234882	1.234875	1.2348698	0.554951	0.554960	0.5549513

In Figure3, the contrasting influences of different parameters on velocity are visually depicted. Figure3 $(a-d)$ shows increasing behaviour of velocity profile with ϕ_1, θ_w, Nr and λ. As NP density and their interaction with fluid particles both strengthen with the elevation in (ϕ_1) volume proportion in the working fluid, results in velocity enhancement. With elevation in θ_w (T_w / T_∞) the velocity profile shows increasing trend. As Nr surge, the radiative heat transfer rate within the Hnf raised, results in enhancing its momentum. The transition of the local buoyancy parameter (λ) from negative to positive values corresponds to a gradual strengthening of buoyancy forces, resulting in intensified fluid motion and increased flow velocities.

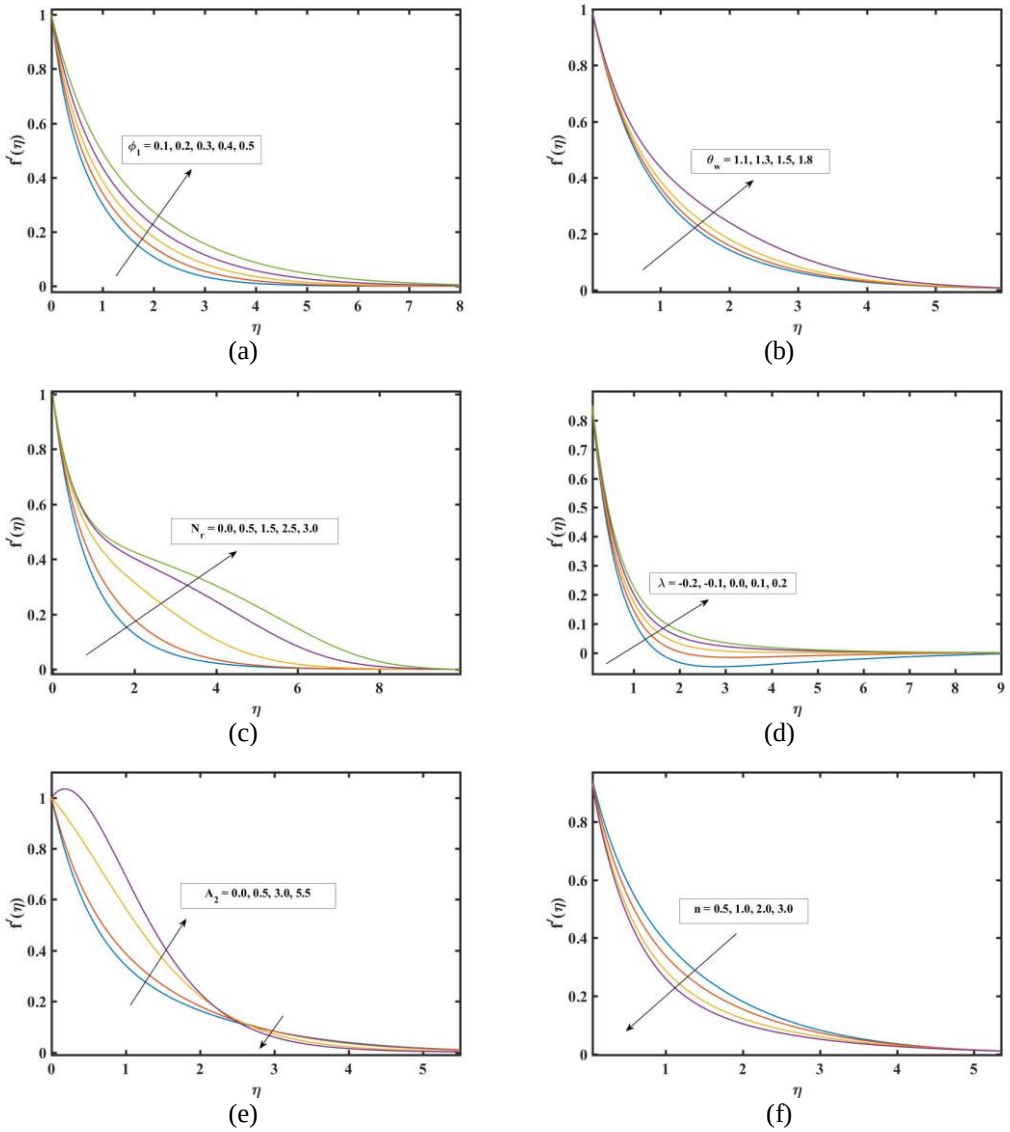

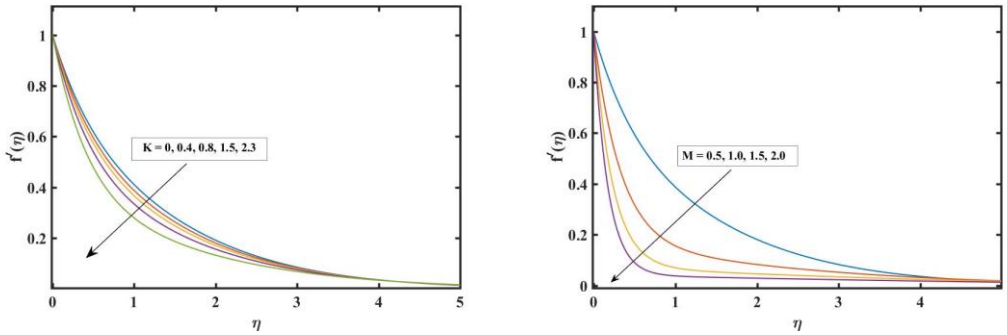

(g) (h)

Figure 3: The contrast in $f^{'}$ against **(a)** ϕ_1, **(b)** θ_w, **(c)** Nr, **(d)** n, **(e)** λ, **(f)** A_2, **(g)** K and **(h)** M

In Figure 3 (e), the velocity profile shows incline nature at upper boundary and decline at lower surface as A_2 inherently remains non-negative, its elevation results in greater non-linear thermal expansion coefficients, augmenting fluid velocity near the surface through intensified thermal buoyancy effects and decrease even A_2 escalates due to reduced temperature gradients toward the free stream. Figure 3 (f-h) demonstrates a declining trend in the velocity profile with n, K and M respectively. An upsurge in the parameter n is accompanied by decline in the velocity factor. Consequently, the thinning in boundary layer of momentum as n increases is noted. Increasing values of K result in higher porosity, enabling a greater volume of fluid to pass through the pores within the medium rather than along its surface. This diversion of flow away from the boundary layer results in a reduction in velocity. directly adjacent to the solid surface. With escalation in M, the magnetic field strength intensifies, thereby amplifying its retarding impact on fluid velocity. The resultant Lorentz force, perpendicular to the flow, hinders fluid motion within the boundary layer. Consequently, as M value elevate, Hnf's velocity profile undergoes a substantial decrease.

Figure 4 (a) illustrates how the temperature profile changes with variations in A_2. With increasing A_2, the temperature decline. In Figure 4 (b), with the increment in the Fr value, thermal profile for Hnf is also recorded to enhance. This happen due to increase in flow resistance to the fluid with increasing Fr which increase heat absorbance. Figure 4 (c) also shows similar trend for K. Figure 4 (d) shows decreasing trend with elevation in λ parameter. With the increasing dominance of the thermal buoyancy force, the fluid's flow rise, consequently leading to a temperature decline. In Figure 4 (e), the dependence of dimensionless temperature on M parameter is demonstrated. As expected, increasing magnetic field intensity acts as a drag force, hindering fluid motion. This restriction translates to a rise in temperature due to viscous dissipation with thermal boundary layer enhancement. Figure 4 (f-i) demonstrated elevation in temperature with n, Nr, ϕ_1 and θ_w respectively. Due to the impact of these parameters, the fluid experiences a reduction in thermal diffusivity, leading to a rise in temperature.

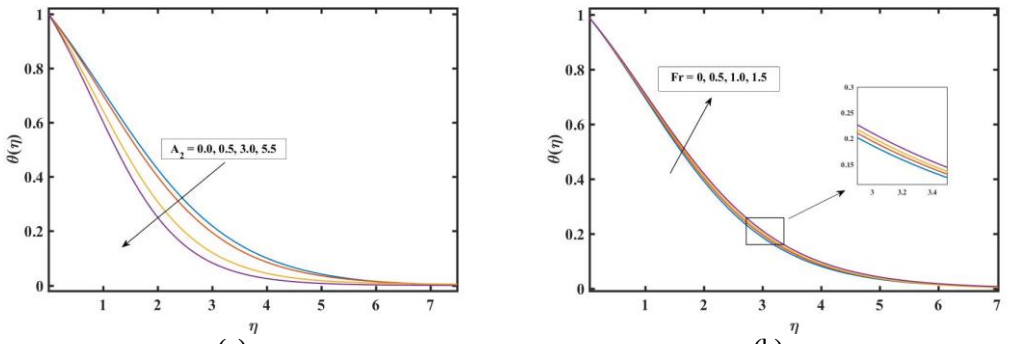

(a)

(b)

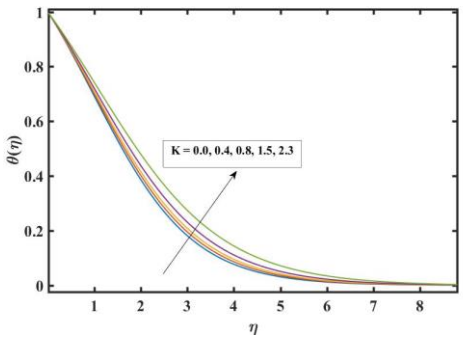

(c)

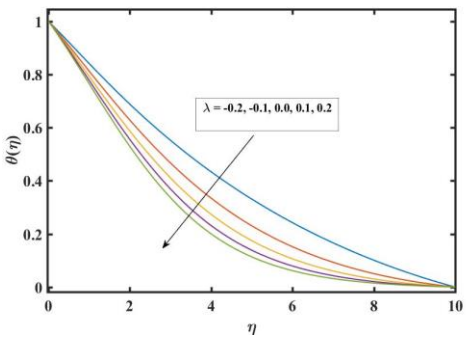

(d)

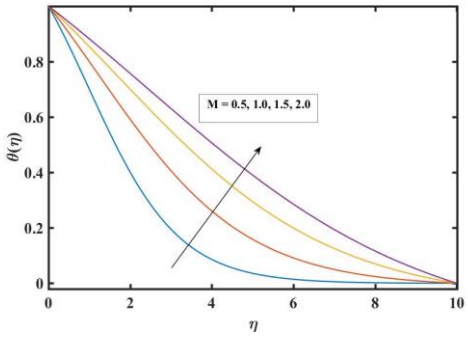

(e)

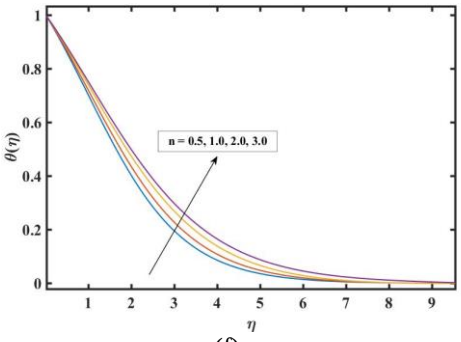

(f)

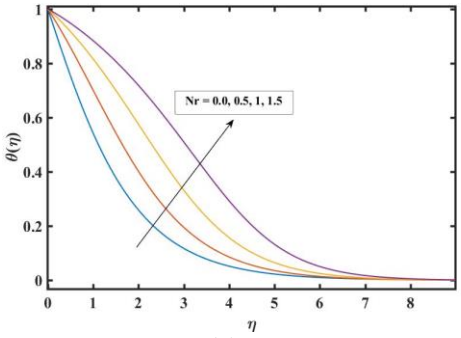

(g)

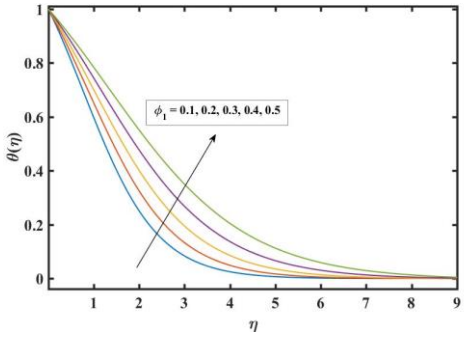

(h)

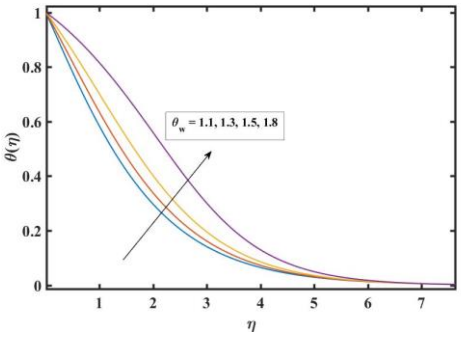

(i)

Figure 4: The contrast in θ against **(a)** A_2, **(b)** Fr, **(c)** K, **(d)** λ, **(e)** M, **(f)** n, **(g)** Nr, **(h)** ϕ_1 and **(i)** θ_w

Nusselt number generally represent the heat reansfer rate from boundary to the fluid. Figure 5 (a) suggests that both A_2 and n aligns with the classical concept that enhanced convection leads to better heat transfer, signifying improved heat transport efficacy between the heated surface to the fluid. Such enhancements are typically desirable across a range of heat transfer applications. With the influence of ϕ_1, Figure 5 (b) marked reduced Nusselt number value. Figure 5 (c) illustrates influence of ϕ_1 and θ_w on heat transmission rate. It is noted that with increaing in both ϕ_1 and $theta_w$, Nusselt number decrease. With augmentation of λ and K in Figure 5 (d), heat transfer rate enhance with λ, while K opposes λ. Figure 5 (e) demonstrated reduction in Nusselt number with M whereas λ tries to improve the overall heat transmission. Figure 5 (f) depicted influence of Pr and K on heat transfer rate, which show enhancement for increasing Pr but decreasing wiith K augmentation.

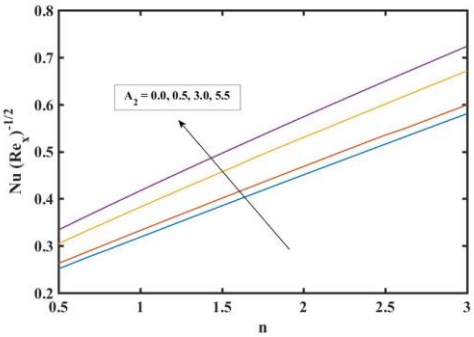

(a)

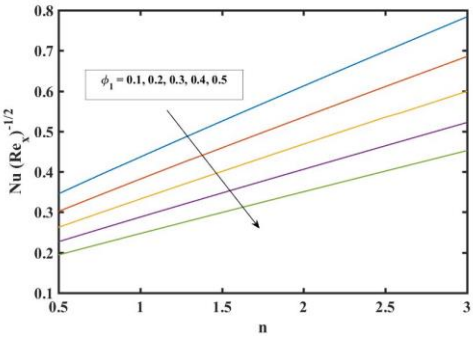

(b)

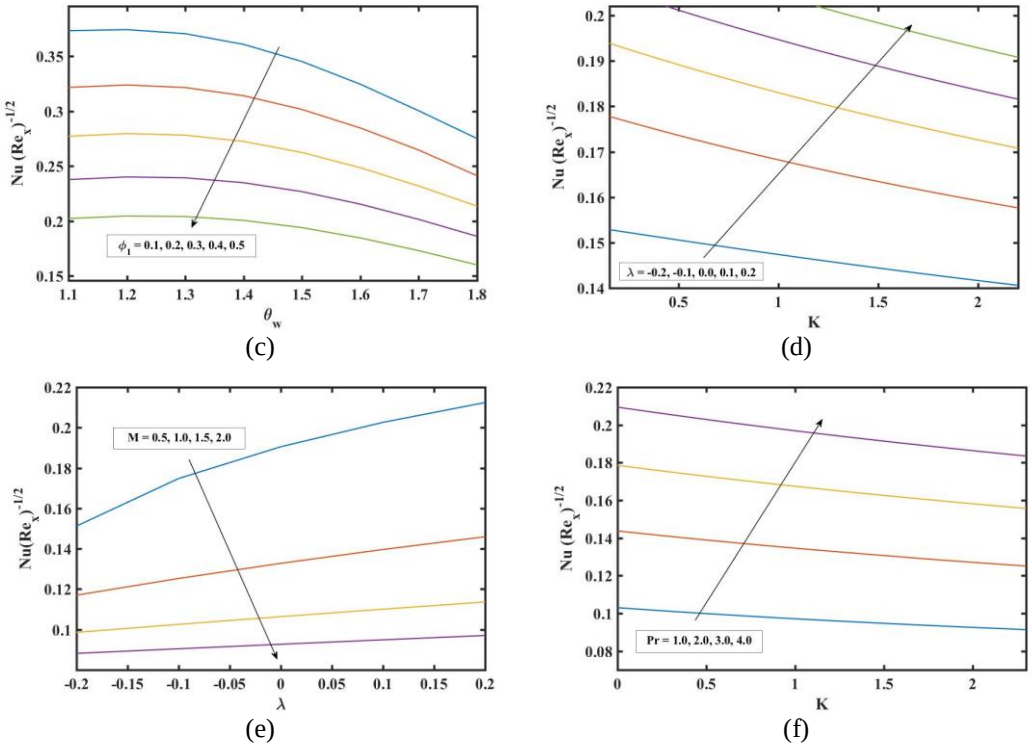

Figure 5: The contrast in $Nu(Re_x)^{-1/2}$ against **(a)** A_2, **(b,c)** ϕ_1, **(d)** λ, **(e)** M and **(f)** Pr

Figure 6 (a-f) depicted the alteration of skin friction coefficient with distinct parameters θ_w, K, M, ϕ_1, λ and Fr. Figure 6 (a) displayed $Cf(Re_x)^{1/2}$ against K with shifting θ_w value, revealing enhancement in rate of shear stress with θ_w elevation and lowered with K. Figure 6 (b) exhibited decrease in $Cf(Re_x)^{1/2}$ with increasing parameter M and increase in drag with inclination of ϕ_1. Figure 6 (c) also showed same trend for $Cf(Re_x)^{1/2}$ with varying M plotted against λ. $Cf(Re_x)^{1/2}$ is found to reduce in Figure 6 (d) for augmented K, potentially indicating improved fluid performance or efficiency in heat exchange while amplify in Figure 6 (e) with λ influence plotted against M. Figure 6 (f) portrayed rate of shear stress against ϕ_1 for Fr and found depletion with Fr influence.

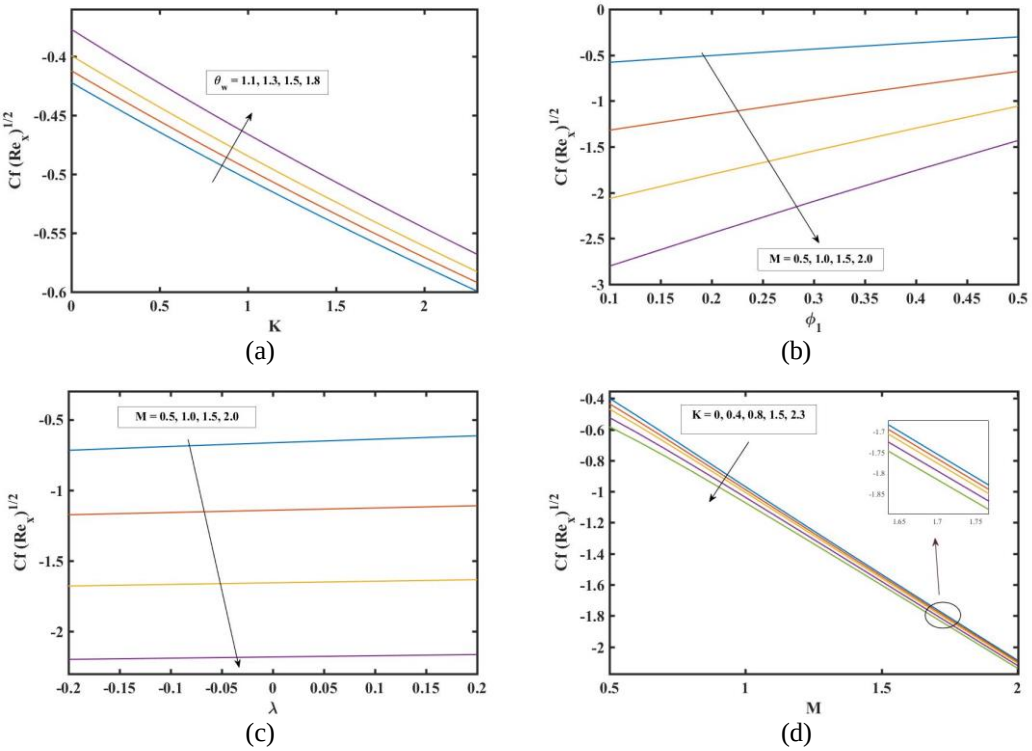

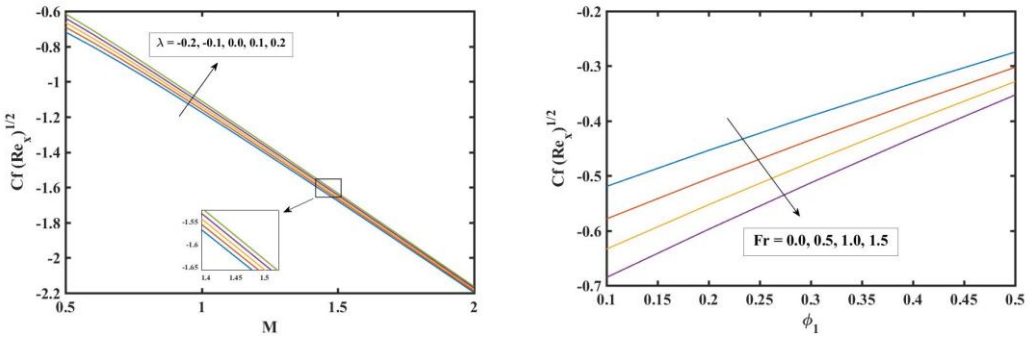

(e) (f)

Figure 6: The contrast in $Cf\,(Re_x)^{1/2}$ against **(a)** θ_w, **(b,c)** M, **(d)** K, **(e)** λ and **(f)** Fr

Table 4 represents variation in heat transmission rates for various parameters for sphere (r = 3), brick (r = 3.7) and platelet (r = 5.7) shaped Hnf. The table depicted that the heat transfer rate is higher for spherical shape followed by brick and platelet shape.

Table 4 Numerical findings regarding heat transfer rates for varying values of absorbed parameters

M	K	A_2	Nr	ϕ_1	n	Fr	λ	θ_w	$GO+Ag/H_2O$ $(r=3)$	$GO+Ag/H_2O$ $(r=3.7)$	$GO+Ag/H_2O$ $(r=5.7)$
0.5	0.4	0.5	0.5	0.3	0.5	0.5	1.0	1.5	0.2623	0.2329	0.1760
1.0									0.1842	0.1619	0.1216
1.5									0.1382	0.1224	0.0954
2.0									0.1129	0.1016	0.0826
0.5	0.8								0.2566	0.2275	0.1716
	1.5								0.2474	0.2190	0.1647
		3.0							0.2903	0.2605	0.2014
	0.4								0.3044	0.2738	0.2127
		5.5							0.3336	0.3016	0.2371
1.0		0.5	1						0.1689	0.1518	0.1184
0.5									0.2453	0.2221	0.1736
			1.5						0.2148	0.1982	0.1597
			0.5	0.1					0.3453	0.3190	0.2616
				0.2					0.3016	0.2725	0.2127
				0.4					0.2267	0.1984	0.1471
				0.5					0.1939	0.1680	0.1237
				0.3	1.0				0.3323	0.2936	0.2198
					3.0				0.5991	0.5239	0.3851
					0.5	1.0			0.2585	0.2293	0.1730
						1.5			0.2545	0.2257	0.1703
						0.5	2.0		0.2987	0.2680	0.2069
							1.0	2.5	0.1017	0.0953	0.0799

Conclusion

This article investigates the flow of a Hnf over a non-linearly stretched surface, incorporating silver and graphene oxide NPs, while considering non-linear thermal radiation and mixed convection effects within a porous medium. Key discoveries from this study include:

- The velocity and temperature profile enhance with increasing GO NPs concentration, leads to betterment in heat transfer applications.
- Non-linear thermal radiation (N_r) shows positive approach to enhance velocity for Hnf.
- Thermal conductivity found to reduce with elevation in non-linear convection and buoyancy parameter respectively.
- Skin friction coefficient lowered with elevation in magnetic filed and porosity parameter.
- Spherical NPs offer the most advantageous heat transfer rate among the investigated shapes.

.

References

[1] Afzal, S., Qayyum, M., Riaz, M. B., and Wojciechowski, A. (2023). Modeling and simulation of blood flow under the influence of radioactive materials having slip with mhd and nonlinear mixed convection. Alexandria Engineering Journal, 69:9–24.

[2] Ahammed, N., Asirvatham, L. G., and Wongwises, S. (2016). Thermo electric cooling of electronic devices with nanofluid in a multiport mini channel heat exchanger. Experimental Thermal and Fluid Science, 74:81–90.

[3] Ali, K., Faridi, A. A., Ahmad, S., Jamshed, W., Hussain, S. M., and Tag-Eldin, E. S. M. (2022). Quasi-linearization analysis for entropy generation in mhd mixed-convection flow of casson nanofluid over nonlinear stretching sheet with arrhenius activation energy. Symmetry, 14(9):1940.
[4] Ashlin, T. and Mahanthesh, B. (2019). Exact solution of non-coaxial rotating and non-linear convective flow of cu–al2o3–h2o hybrid nanofluids over an infinite vertical plate subjected to heat source and radiative heat. Journal of Nanofluids, 8(4):781–794.
[5] Bhatti, M., Khalique, C., Bég, T. A., Bég, O. A., and Kadir, A. (2020). Numerical study of slip and radiative effects on magnetic fe3o4-water-based nanofluid flow from a nonlinear stretching sheet in porous media with soret and dufour diffusion. Modern Physics Letters B, 34(02):2050026.
[6] Chandel, S. and Sood, S. (2022). Unsteady flow of williamson fluid under the impact of prescribed surface temperature (pst) and prescribed heat flux (phf) heating conditions over a stretching surface in a porous enclosure.
[7] Choi, S. U. and Eastman, J. A. (1995). Enhancing thermal conductivity of fluids with nanoparticles. Technical report, Argonne National Lab.(ANL), Argonne, IL (United States).
[8] Cortell, R. (2007). Viscous flow and heat transfer over a nonlinearly stretching sheet. Applied Mathematics and Computation, 184(2):864–873.
[9] Eastman, J. A., Choi, S., Li, S., Yu, W., and Thompson, L. (2001). Anomalously increased effective thermal conductivities of ethylene glycol-based nanofluids containing copper nanoparticles. Applied physics letters, 78(6):718–720.
[10] Eid, M. R., Mahny, K. L., Muhammad, T., and Sheikholeslami, M. (2018). Numerical treatment for carreau nanofluid flow over a porous nonlinear stretching surface. Results in physics, 8:1185–1193.
[11] Fenuga, O. J., Hassan, A. R., and Olanrewaju, P. O. (2020). Effects of radiation and eckert number on mhd flow with heat transfer rate near a stagnation point over a non-linear vertical stretching sheet. International Journal of Applied Mechanics and Engineering, 25(1):27–36.
[12] Haider, F., Hayat, T., and Alsaedi, A. (2021). Flow of hybrid nanofluid through darcy-forchheimer porous space with variable characteristics. Alexandria Engineering Journal, 60(3):3047–3056.
[13] Hayat, T., Haider, F., and Alsaedi, A. (2020a). Darcy-forchheimer flow with nonlinear mixed convection. Applied Mathematics and Mechanics, 41:1685–1696.
[14] Hayat, T., Haider, F., Muhammad, T., and Alsaedi, A. (2020b). Darcy-forchheimer flow by rotating disk with partial slip. Applied Mathematics and Mechanics, 41:741–752.
[15] Hayat, T. and Nadeem, S. (2017). Heat transfer enhancement with ag–cuo/water hybrid nanofluid. Results in physics, 7:2317–2324.
[16] Jana, S., Salehi-Khojin, A., and Zhong, W.-H. (2007). Enhancement of fluid thermal conductivity by the addition of single and hybrid nano-additives. Thermochimica acta, 462(1-2):45–55.
[16] Javadi, F. S., Sadeghipour, S., Saidur, R., BoroumandJazi, G., Rahmati, B., Elias, M., and Sohel, M. (2013). The effects of nanofluid on thermophysical properties and heat transfer characteristics of a plate heat exchanger. International Communications in Heat and Mass Transfer, 44:58–63.
[17] Karaaslan, I. and Menlik, T. (2021). Numerical study of a photovoltaic thermal (pv/t) system using mono and hybrid nanofluid. Solar Energy, 224:1260–1270.
[18] Khan, M. R., Pan, K., Khan, A. U., and Nadeem, S. (2020). Dual solutions for mixed convection flow of sio2-al2o3/water hybrid nanofluid near the stagnation point over a curved surface. Physica A: Statistical Mechanics and its Applications, 547:123959.
[19] Khan, U., Zaib, A., Bakar, S. A., and Ishak, A. (2021). Stagnation-point flow of a hybrid nanoliquid over a non-isothermal stretching/shrinking sheet with characteristics of inertial and microstructure. Case Studies in Thermal Engineering, 26:101150.
[20] Kierzenka, J. and Shampine, L. F. (2001). A bvp solver based on residual control and the maltab pse. ACM Transactions on Mathematical Software (TOMS), 27(3):299–316.
[21] Mahanthesh, B., Animasaun, I., Rahimi-Gorji, M., and Alarifi,I. M. (2019). Quadratic convective transport of dusty casson and dusty carreau fluids past a stretched surface with nonlinear thermal radiation, convective condition and non-uniform heat source/sink. Physica A: Statistical Mechanics and its Applications, 535:122471.
[22] Maiga, S. E. B., Nguyen, C. T., Galanis, N., and Roy, G. (2004). Heat transfer behaviours of nanofluids in a uniformly heated tube. Super lattices and Microstructures, 35(3-6):543–557.
[23] Mallikarjuna, H. B., Nirmala, T., Punith Gowda, R. J., Manghat, R., and Varun Kumar, R. S. (2021). Two-dimensional darcy–forchheimer flow of a dusty hybrid nanofluid over a stretching sheet with viscous dissipation. Heat Transfer, 50(4):3934–3947.
[24] Masood, S., Farooq, M., and Anjum, A. (2021). Influence of heat generation/absorption and stagnation point on polystyrene–tio2/h2o hybrid nanofluid flow. Scientific Reports, 11(1):22381.
[25] Modi, K., Patel, P., and Patel, S. (2023). Applicability of mono-nanofluid and hybrid-nanofluid as a technique to improve the performance of solar still: A critical review. Journal of Cleaner Production, 387:135875.
[26] Mukherjee, S., Mishra, P. C., and Chaudhuri, P. (2018). Stability of heat transfer nanofluids–a review. ChemBioEng Reviews, 5(5):312–333.
[27] Mustafa, M. and Khan, J. A. (2015). Model for flow of casson nanofluid past a non-linearly stretching sheet considering magnetic field effects. AIP advances, 5(7).
[28] Nadeem, S., Abbas, N., and Malik, M. (2020). Inspection of hybrid based nanofluid flow over a curved surface. Computer methods and programs in biomedicine, 189:105193.
[29] Nagarajan, P., Subramani, J., Suyambazhahan, S., and Sathyamurthy, R. (2014). Nanofluids for solar collector applications: a review. Energy Procedia, 61:2416–2434.
[30] Nandeppanavar, M. M., MC, K., and N, R. (2023). Effect of non-linear thermal radiation on the stagnation point flow of double diffusive free convection due to moving vertical plate. Journal of Engineering, Design and Technology, 21(1):150–166.
[31] Pandey, A. K., Bhattacharyya, K., Gautam, A. K., Rajput, S., Mandal, M. S., Chamkha, A. J., and Yadav, D. (2023). Insight into the relationship between non-linear mixed convection and thermal radiation: The case of newtonian fluid flow due to non-linear stretching. Propulsion and Power Research, 12(1):153–165.

[32] Puneeth, V., Manjunatha, S., Madhukesh, J., and Ramesh, G. (2021). Three dimensional mixed convection flow of hybrid casson nanofluid past a non-linear stretching surface: A modified buongiornos model aspects. Chaos, Solitons & Fractals, 152:111428.
[33] Ramzan, M., Dawar, A., Saeed, A., Kumam, P., Watthayu, W., and Kumam, W. (2021). Heat transfer analysis of the mixed convective flow of magneto hydrodynamic hybrid nanofluid past a stretching sheet withvelocity and thermal slip conditions. Plos one, 16(12):e0260854.
[34] Sadiq, M. A. and Hayat, T. (2016). Darcy–forchheimer flow of magneto maxwell liquid bounded by convectively heated sheet. Results in physics, 6:884–890.
[35] Sheikholeslami, M., Hatami, M., and Ganji, D. (2014). Nanofluid flow and heat transfer in a rotating system in the presence of a magnetic field. Journal of Molecular liquids, 190:112–120.
[36] Singh, B. and Sood, S. (2024). Hybrid nanofluids preparation, thermo-physical properties, and applications: A review. Hybrid Advances, page 100192.
[37] Singh, D., Toutbort, J., Chen, G., et al. (2006). Heavy vehicle systems optimization merit review and peer evaluation. Annual Report, Argonne National Laboratory, 23:405–411.
[38] Srinivasacharya, D.andSurender, O.(2015). Double stratification effects on mixed convection along a vertical plate in a non-darcy porous medium. Procedia Engineering, 127:986–993.
[39] Suresh, S., Venkitaraj, K., Selvakumar, P., and Chandrasekar, M. (2011). Synthesis of al2o3–cu/water hybrid nanofluids using two step method and its thermo physical properties. Colloids and Surfaces A: Physicochemical and Engineering Aspects, 388(1-3):41–48.
[40] Thakur, A. and Sood, S. (2023). Tri-hybrid nanofluid flow towards convectively heated stretching riga plate with variable thickness. Journal of Nanofluids, 12(4):1129–1140.
[41] Turcu, R., Darabont, A., Nan, A., Aldea, N., Macovei, D., Bica, D., Vekas, L., Pana, O., Soran, M., Koos, A., et al. (2006). New polypyrrole-multiwall carbon nanotubes hybrid materials. Journal of optoelectronics and advanced materials, 8(2):643–647.
[42] Wong, K. V. and De Leon, O. (2010). Applications of nanofluids: current and future. Advances in mechanical engineering, 2:519659.
[43] Xu, Q., Yang, G., Jia, S., Wang, Z., Akkurt, N., Zhang, H., Zhou, Q., Shen, M., Yang, D., Zhu, L., et al. (2022). Experimental study on synergistic enhancement of thermal performance of a closed two-phase thermosyphon by a tio2 nanofluid doped with al2o3. Case Studies in Thermal Engineering, 36:102192.
[45] Xuan, Y. and Li, Q. (2000). Heat transfer enhancement of nanofluids. International Journal of heat and fluid flow, 21(1):58–64.
[46] Zainal, N. A., Nazar, R., Naganthran, K., and Pop, I. (2021). Stability analysis of mhd hybrid nanofluid flow over a stretching/shrinking sheet with quadratic velocity. Alexandria Engineering Journal, 60(1):915–926.